ROYAL SOCIETY
OF CHEMISTRY

EDGE ARTICLE

Check for updates

Constrained TACC3 peptidomimetics for a non-canonical protein–protein interface elucidate allosteric communication in Aurora-A kinase†

Diana Gimenez, [ID] [a] Martin Walko, [ID] [bd] Jennifer A. Miles, [ID] [cd] Richard Bayliss, [ID] *[cd]
Megan H. Wright [ID] *[bd] and Andrew J. Wilson [ID] *[abd]

Peptidomimetic design for non-canonical interfaces is less well established than for α-helix and β-strand mediated protein–protein interactions. Using the TACC3/Aurora-A kinase interaction as a model, we developed a series of constrained TACC3 peptide variants with 10-fold increased binding potencies (K_d) towards Aurora-A in comparison to the parent peptide. High-affinity is achieved in part by restricting the accessible conformational ensemble of the peptide leading to a more favourable entropy of binding. In addition to acting as potent orthosteric TACC3/Aurora-A inhibitors, these peptidomimetics were shown to activate the kinase and inhibit the N-Myc/Aurora-A interaction at a distal site. Thus, the potency of these tools uniquely allowed us to unveil new insight into the role of allosteric communication in the kinase.

1 Introduction

Protein–protein interactions (PPIs) play a crucial mechanistic role in regulating health and disease biology.[1,2] PPIs thus represent important targets in drug discovery.[3] Competitive/orthosteric PPI inhibition has been historically challenging given that protein–protein interfaces are relatively large and lack the well-defined pockets that are characteristic of traditional drug targets.[4,5] Although success has been achieved using fragment-based approaches, small-molecules developed from screening libraries and computational methods,[6] there remains a need to develop new enabling methods and modalities for PPI modulation. Peptides are attractive given they offer functionally optimal molecular recognition properties.[7,8] Significant efforts have been invested in developing peptidomimetic inhibitors of α-helix mediated PPIs, with cyclization employed as a tool to bias a given peptide toward its bioactive conformation, suppress proteolysis, and improve cell uptake.[9] Emerging studies extend this approach to β-strand[10–12] and loop[13] mediated PPIs, whilst screening tools have yielded cyclic and bicyclic peptides for a range of other targets.[14,15] However, strategies for the design of constrained peptides that mimic non-canonical secondary structures are less

well developed. Whilst general principles to "pre-organise" irregular structures have to be elaborated, hydrophobic cross-links that replace crucial ExoS residues involved in 14-3-3 binding were rationally introduced and optimized to stabilize an irregular bound peptide structure.[16] Herein, we used rational design to develop a peptidomimetic inhibitor of the TACC3/Aurora-A interaction. Judicious incorporation of non-natural amino acids and constraints led to a peptide with enhanced affinity for its target as a consequence of excluding accessible conformations thus raising the ground state energy of the conformational ensemble. The power of these peptidomimetic tools to understand the target protein is illustrated through experiments showing that they activate Aurora-A kinase and inhibit a further PPI (N-Myc/Aurora-A) at a remote site.

2 Results and discussion

Aurora-A is a Ser/Thr protein kinase that plays an essential role in mitosis.[17] Aberrant Aurora-A function is associated with cancer development and progression making it an attractive drug discovery target. However, despite entry of numerous active site Aurora-A inhibitors into clinical trials,[18–21] none have progressed to clinical use. This might arise due to on-target toxicity associated with the essential function of Aurora-A[22,23] but also because of Aurora-A functions that are independent of its intrinsic kinase activity.[24,25] This means that active site kinase inhibitors might not suffice to achieve therapeutic efficacy. As an incomplete kinase, Aurora-A function and localization is regulated through recognition of a plethora of clients. Among those it recruits and phosphorylates is Transforming Acidic Coiled-Coil Containing Protein 3 (TACC3). TACC3 is instrumental for spindle assembly and chromosome

[a]School of Chemistry, University of Birmingham, Edgbaston, Birmingham B15 2TT, UK. E-mail: a.j.wilson.1@bham.ac.uk

[b]School of Chemistry, University of Leeds, Woodhouse Lane, Leeds LS2 9JT, UK. E-mail: M.H.Wright@leeds.ac.uk

[c]School of Molecular and Cellular Biology, University of Leeds, Woodhouse Lane, Leeds LS2 9JT, UK. E-mail: R.W.Bayliss@leeds.ac.uk

[d]Astbury Centre for Structural Molecular Biology, University of Leeds, Woodhouse Lane, Leeds LS2 9JT, UK

segregation in mammalian cells, playing a central role in achieving microtubule stabilization during mitosis through its interaction with chTOG/XMAP215.[26,27] TACC3 is mutated and overexpressed in different cancer types, including glioblastoma, with its fusion products also exerting oncogenic activity.[28,29] Moreover, depletion or pharmacological inhibition of Aurora-A kinase activity by small-molecule inhibitors has been shown to disrupt centrosomal localization of TACC3,[30] and suppress tumor growth,[31] whilst siRNA-mediated TACC3 depletion leads to a similar phenotype to that which occurs through Aurora-A active-site inhibition.[32,33]

Burgess et al. reported an X-ray crystal structure for a fragment of TACC3 (residues 519–563) bound to Aurora-A$_{122-403}$ $_{C290A/C393A/D274N}$ (PDB: 5ODT; Fig. 1a).[26] The TACC3 fragment was shown to adopt an extended conformation with two short regions adopting secondary structure: a 3_{10}-helical turn (residues 527–531), and an α-helix (residues 546–555, the αTR domain, Fig. 1a). Fluorescence anisotropy (FA) titrations established that TACC3$_{522-536}$ – encompassing the 3_{10}-helical turn – makes the dominant contribution to Aurora-A affinity (∼10–20 μM).[27] Microscale thermophoresis further identified Phe525^{TACC3} as a hot-spot residue for Aurora-A binding. Moreover, HeLa cells that express a F525A variant of TACC3 generated using CRISPR-Cas9 exhibited a phenotype consistent with critical roles of this hot-spot in early and late mitosis.[26,27]

Our first objective was to optimize the affinity of TACC3$_{522-536}$ for Aurora-A. Our analyses of the TACC3/Aurora-A co-crystal structure identified three interactions that might play a role in influencing the affinity of TACC3 for Aurora-A:

a charge-reinforced hydrogen-bond between Glu523^{TACC3} and Arg137$^{Aurora-A}$; a hydrophobic contact between Leu532^{TACC3} and Tyr148$^{Aurora-A}$; and, a cation–π interaction between Phe525^{TACC3} and Arg151$^{Aurora-A}$. These analyses were supported through in silico alanine scanning (Table S1†).[34]

2.1 Sequence variation leads to optimization of the Phe525^{TACC3} interaction with Aurora-A

We hypothesized that para-substituted phenylalanine analogs able to occupy an increased volume within the Phe525^{TACC3} binding pocket (Leu149$^{Aurora-A}$, Ile158$^{Aurora-A}$, Arg151$^{Aurora-A}$) could enhance solvophobic packing and modulate the strength of the Phe525-^{TACC3}/Arg151$^{Aurora-A}$ cation–π interaction (Fig. 1c). We prepared a series of TACC3$_{522-536}$ variants where a variety of unnatural phenylalanine analogs were incorporated in place of the naturally occurring Phe525^{TACC3} (Fig. 2). Their IC$_{50}$ values (Fig. 2, S1 and Table S2†) were then determined through competition FA experiments against the fluorescently labeled TACC3$_{522-536}$ WT sequence bound to Aurora-A$_{122-403-C290A/C393A}$. Compared to the WT peptide (IC$_{50}$ = 163 ± 13 μM), up to ∼5-fold enhanced inhibitory potencies for three of the variants based on simple halogen para-substituted analogs were observed: TACC3$_{522-536-(4-Cl)525F}$ (IC$_{50}$ = 46 ± 8 μM), TACC3$_{522-536-(4-Br)525F}$ (IC$_{50}$ = 34 ± 6 μM) and TACC3$_{522-536-(4-I)525F}$ (IC$_{50}$ = 34 ± 3 μM). For the smaller (4-F)^{525}Phe variant no improvement was observed, indicating that both the halogen-atom size and electronic properties play a role in enhancing affinity towards Aurora-A. To provide further insight on the improved affinities, molecular dynamics (MD) analyses were
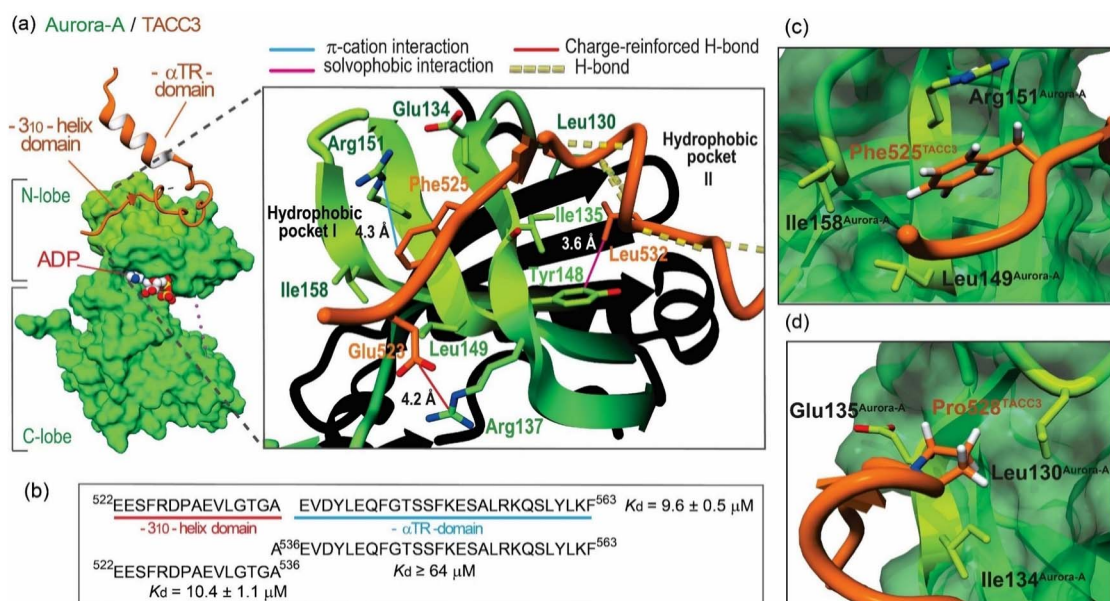

Fig. 1 Key features of the TACC3/Aurora-A complex: (a) crystal structure of the Aurora-A$_{122-403-C290A/C393A/D274N}$ catalytic domain (forest-green) in complex with TACC3$_{522-563}$ (orange; PDB: 5ODT), magnified view of the TACC3/Aurora-A PPI interface with key residues shown as sticks, and TACC3 hot-spot residues highlighted; (b) sequence of TACC3 docking region to Aurora-A, TACC3$_{522-563}$, and individual dissociation constants (K_d) for each domain as measured by FA direct binding assays. K_d values are given as the mean value and corresponding standard deviation (SD) from triplicate titrations of Aurora-A$_{122-403-C290A/C393A}$ in the presence of the corresponding FAM-labeled peptides (50 nM) (n = 3); (c) magnified view of the MD calculated energy minimum structure of WT TACC3$_{522-536}$ (in orange) in the presence of Aurora-A, showing the arrangement around the key Phe525^{TACC3}; (d) of the MD calculated energy minimum structure of WT TACC3$_{522-536}$ (in orange) in the presence of Aurora-A, showing the exo-pucker conformation and arrangement of Pro528^{TACC3}.
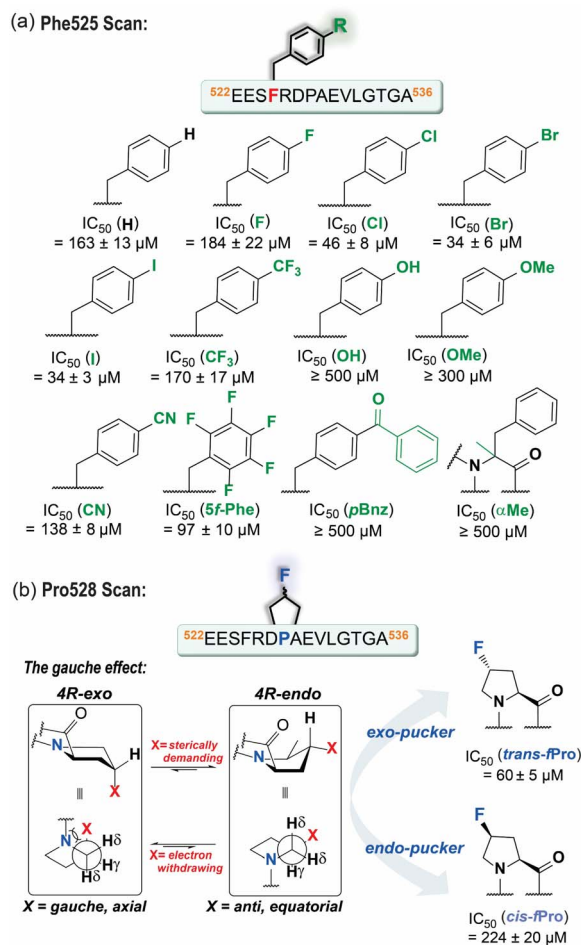
Fig. 2 Single-point amino-acid modification: (a) sequence and chemical structure of the different Phe525 analogs tested and their corresponding competition FA IC_{50} values; (b) schematics illustrating the gauche effect in fluoro-prolines and the corresponding competition FA IC_{50} values assessed for the TACC3$_{522-536}$ variants carrying these modifications. All IC_{50} values are reported as the average value $\pm$ SD of triplicate competition experiments ($n = 3$) against 200 nM FAM-Ahx-TACC3$_{522-536}$ at 25 °C in 25 mM Tris, 150 mM NaCl, 5 mM MgCl$_2$, pH 7.5, using 5 μM Aurora-A$_{122-403-C290A/C393A}$.

carried out by modelling the WT and the iodinated variant (TACC3$_{522-536-(4-I)525F}$) in complex with Aurora-A (Fig. S2–S7†). The calculated minimum energy structures were consistent with deeper insertion of (4-I)Phe525^{TACC3} into its hydrophobic pocket on Aurora-A (see Fig. S5–S7†). Additionally, MD analyses of the number of contacts per-residue between TACC3$_{522-536(4-I)525F}$ and the protein over the course of the trajectory indicated increased and more sustained contacts between the iodinated amino acid and Aurora-A (see Fig. S4† *vs.* Fig. S7†). In their minimum energy structures, a shorter distance between Arg151$^{Aurora-A}$ and Phe525-^{TACC3} (3.9 Å for (4-I)Phe525 *vs.* 4.2 Å for Phe525) is consistent with a stronger cation–π interaction.

2.2 A non-natural amino acid promotes conformational selection at the Pro528^{TACC3} residue

MD analyses alongside *in silico* alanine scanning[34] were instrumental in examining additional residues for further

optimization (Fig. 2, S2–S4 and Table S1†). Both analyses indicated that when bound to Aurora-A, residues: Val531^{TACC3} ($\Delta\Delta G_{pred} = 3.6$ kJ mol^{-1}), Leu532^{TACC3} ($\Delta\Delta G_{pred} = 8.2$ kJ mol^{-1}) and Pro531^{TACC3} ($\Delta\Delta G_{pred} = 4.8$ kJ mol^{-1}) are important for binding and establish a significant number of contacts with the surface of Aurora-A (Fig. S4†). We also observed in the energy minimum structure of the complex, that Pro531^{TACC3} exhibits a C$^{\gamma}$-*exo*-pucker conformation, which likely facilitates deeper insertion of the side-chain into a hydrophobic pocket on Aurora-A (Leu130$^{Aurora-A}$, Ile134$^{Aurora-A}$ and Glu135$^{Aurora-A}$ Fig. 1d and S2†). The *exo*-pucker conformation at the proline residue allows a peptidyl-prolyl *trans*-amide bond of the preceding residue, which favors the accommodation and propagation of the TACC3 backbone chain across the surface of Aurora-A.

We assessed the effects of sequence variation at Leu532^{TACC3} and Val531^{TACC3} by replacing them with isoleucine or norleucine (nLeu). However, poor tolerance to these modifications was observed (TACC3$_{522-536-L532nL}$ $IC_{50} = 213 \pm 16$ μM, TACC3$_{522-536-V531I}$ $IC_{50} \geq 300$ μM, TACC3$_{522-536-V531nL}$ $IC_{50} \geq 300$ μM *vs.* TACC3$_{522-536}$ $IC_{50} = 163 \pm 13$ μM; Fig. S8†).

Exploiting stereo-electronic effects (*i.e.* gauche effect; Fig. 2b) to favor the Pro528 *exo*-pucker conformation observed in the TACC3/Aurora-A structure was more profitable.[35] Incorporation of fluorine has proven effective in controlling the prolyl-ring preference, with *trans*-(4-F)Pro favoring the C$^{\gamma}$-*exo*-pucker conformation at a 6 : 1 ratio, and *cis*-(4-F)Pro biasing the equilibrium to the opposite *endo*-conformer in an estimated 20 : 1 ratio.[36] When TACC3$_{522-536}$ variants based on both possible (4-F) Pro isomers (*i.e. cis* or *trans*-fluoroproline) were tested using competition FA assays (Fig. S9†), we observed that the *exo*-pucker stabilizing *trans*-isomer had ~3-fold increased TACC3/Aurora-A inhibitory potency (TACC3$_{522-536-trans-(4-F)528P}$ $IC_{50} = 60 \pm 5$ μM *vs.* TACC3$_{522-536}$ $IC_{50} = 163 \pm 13$ μM; Fig. 2b). In contrast, incorporation of the *endo*-pucker stabilizing *cis*-(4-F) Pro residue resulted in the opposing effect, reducing the inhibitory potency of the peptide to $IC_{50} \geq 200$ μM. Overall, these data (reinforced with MD simulations on the *trans*-(4-F) Pro variant Fig. S10–S12† for further discussion) demonstrate that the TACC3/Aurora-A interaction is sensitive to the conformation of Pro528^{TACC3} and that inhibitory potency can be tuned using synthetic variation.

2.3 Constraining TACC3 leads to improved inhibitory potency

Although the TACC3/Aurora-A interaction lacks a defined secondary structure, TACC3 becomes more ordered on binding to Aurora-A.[26] We, therefore, explored the use of a maleimide crosslinker to constrain the cysteine variants of the WT peptide between the i and $i+3$ positions to limit the conformational landscape of the peptide and perhaps favor formation of the 3$_{10}$-helical turn observed in the crystal structure (Table S3 and Fig. S13†).[37–39] These variants did not lead to enhanced inhibitory potency (Table S3 and† Fig. S13†).

Better inhibitory potencies were obtained using longer constraints (*i.e.* 4,4′-bis(methyl)biphenyl, Bph) between cysteines introduced at i and $i+6$ positions (Table S3 and

Fig. S13†). To better accommodate such a constraint into the peptide, we also re-explored the TACC3 sequence by truncating and elongating the TACC3$_{522-536}$ peptide. We found TACC3$_{518-532}$, with four additional residues at the N-terminus and four fewer at the C-terminus, to be a suitable template for additional development (Fig. 3a, S14 and Table S4†). This sequence had marginally improved binding potency to Aurora-A when compared to the original TACC3$_{522-536}$ peptide (TACC3$_{518-532}$ $K_d = 7.4$ μM *vs.* TACC3$_{522-536}$ $K_d = 10.4$ μM; Fig. 3a), but more importantly opened up the tactical modification of additional residues not present in the original TACC3$_{522-536}$ sequence.

With the aid of MD analysis on TACC3$_{518-532}$ (Fig. S15–S17†), we identified accessible solvent-exposed L520/R526, K521/D528,

and S524/E530 residue pairs as promising options for introduction of cysteines and then addition of a constraint with a variety of linkers. When these TACC3$_{518-532}$-based variants were tested, up to 4-fold improved IC$_{50}$ values were found for two of the biphenyl-constrained peptides, both showing inhibitory concentrations in the range of IC$_{50} \sim 30$ μM (TACC3$_{518-532-}$ $_{L/R-Bph}$ and TACC3$_{518-532-S/E-Bph}$; Fig. 3b). In comparison, larger IC$_{50}$ values were observed for the corresponding reduced and oxidized species, or when using alternative more flexible, and/or hydrophobic constraints such as octanoyl and polyethylene glycol-based linkers (Table S5, Fig. S18, S19–S22† for MD analyses and discussion).

2.4 Synergistic incorporation of constraints and non-natural amino-acids further improves TACC3 affinity for Aurora-A

With two amino-acid modifications that enhanced binding potency of TACC3 to Aurora-A and two constrained backbones identified, we assessed the extent to which these modifications could be productively combined in a single compound (Fig. 3c). Four modified peptides were assessed: TACC3$_{518-532-L/R-Bph-I}$ and TACC3$_{518-532-L/R-Bph-Br}$ based on the L520C/R526C biphenyl-constrained structure carrying either (4-I)Phe525 or (4-Br) Phe525 modifications, and the corresponding peptides: TACC3$_{518-532-S/E-Bph-I}$ and TACC3$_{518-532-S/E-Bph-Br}$, based on the alternative S524C/E530C constrained template (Fig. S23†). All variants exhibited IC$_{50}$ values of ~20–30 μM against the WT peptide (Fig. S23†). Next, we assessed the effect of incorporating the *trans*-(4-F)Pro528 residue by synthesizing and analyzing the corresponding peptides carrying this modification (TACC3$_{518-532-L/R-Bph-I/fP}$; TACC3$_{518-532-L/R-Bph-Br/fP}$; TACC3$_{518-532-S/E-Bph-I/fP}$ and TACC3$_{518-532-S/E-Bph-Br/fP}$; Fig. 3c, S24, S25 and Table S6†). These variants showed lower IC$_{50}$ values in competition experiments than previous compounds, with all peptides exhibiting IC$_{50}$ values in the range 10–22 ± 2 μM (the limit of sensitivity for the assay). To more accurately assess binding potencies to Aurora-A, we employed direct FA titrations of the protein in the presence of FAM-labelled peptides and assessed their corresponding dissociation constants, K_d. Twelve-fold improved K_d values were measured for the constrained peptides when compared to the linear sequences (Fig. 3c), with all variants showing low micromolar/high nanomolar affinities. MD simulations indicate that these combined modifications act as designed *i.e.* the halogenated phenylalanine better occupies its pocket and the *trans*-fluoroproline favors the *exo*-pucker conformation (Fig. S26–S33†).

Peptide constraints and unnatural amino acids can suppress proteolysis.[40] The L/R constrained peptide exhibited increased resistance to both trypsin (cleavage at positively charged residues) and α-chymotrypsin (cleavage at aromatic and hydrophobic aliphatic residues) whilst the S/E constrained variant was not protected in comparison to the WT sequence, but did exhibit a change in cleavage site (Fig. S34–S40†).

Overall, these results establish the successful complementary incorporation of peptide constraint, unnatural amino acid, and proline conformational control as a means to rationally develop TACC3/Aurora-A inhibitors.
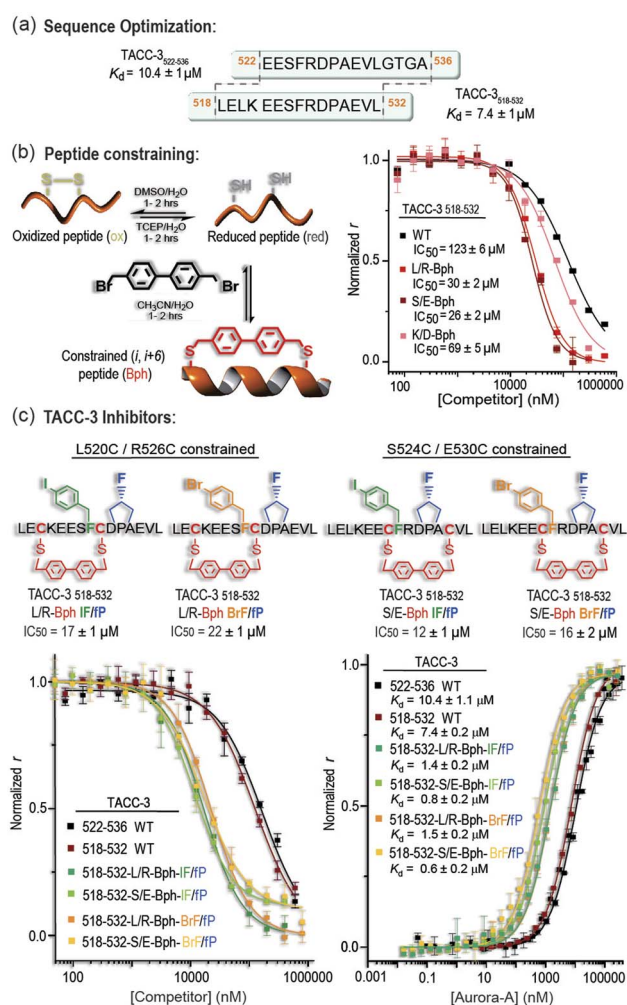

Fig. 3 Novel constrained TACC3/Aurora-A PPI inhibitors: (a) sequence and K_d values measured for WT peptides TACC3$_{522-536}$ and TACC3$_{518-532}$; (b) schematics of peptide constraint; (c) structure of lead Bph-constrained TACC3/Aurora-A PPI inhibitors. (Left lower panel) Competition FA results for lead inhibitors against TACC3$_{522-536}$ WT (5 μM Aurora-A$_{122-403-C290A/C393A}$, 200 nM FAM-Ahx-TACC3$_{522-536}$). (Right lower panel) FA direct titration of FAM-Ahx-inhibitors (50 nM) with Aurora-A$_{122-403-C290A/C393A}$ (all values are given as the average ± SD of a triplicate assay in 25 mM Tris, 150 mM NaCl, 5 mM MgCl$_2$, pH 7.5, 25 °C).

2.5 The constraint restricts the conformational landscape of TACC3 and pre-disposes Phe525 towards Aurora-A binding

To better understand the role of the modifications in increasing the affinity of the TACC3 peptidomimetics towards Aurora-A, we studied their unbound solution structure by NMR spectroscopy (Fig. 4). At 5 °C, we found that TACC3$_{518-532}$ showed well-resolved ^{1}H resonances (Fig. 4a, S41–S49 and Table S7†), exhibiting amide-bond N–H vicinal coupling constants for each residue, $^3J_{NH–\alpha H}$, persistently in the range of 6–7 Hz, consistent with a general disordered/random coil secondary structure.[41] Analysis of TACC3$_{518-532}$ based on recently published random-coil chemical shifts for disordered proteins $(\Delta\delta_{RC})$[42] supported this conclusion; both Cα $(\Delta\delta_{C\alpha})$ and Hα $(\Delta\delta_{H\alpha})$ secondary chemical shifts showed extended regions with small negative values $(|\Delta\delta_{C\alpha}| \leq 1$ ppm; $|\Delta\delta_{H\alpha}| \leq 0.25$ ppm), much lower and for $\Delta\delta_{H\alpha}$ of opposing sign, to those of α-helical structures $(\Delta\delta_{C\alpha} \geq 2.0$–3.5 ppm; Table S8,† Fig. S50–S52†).[43,44] We found no evidence of a folded (helical) structure in solution when the corresponding TOCSY/NOESY spectra were analyzed; only correlations between consecutive $(i, i-1)$ amide bonds were observed. Modified peptide TACC3$_{518-532-L/R-Bph-IF/fP}$, exhibited broadened ^{1}H resonances of lower intensity, in particular for the constrained Bph group, residues Cys526^{TACC3}, Glu523^{TACC3}, and (4-I)Phe525^{TACC3} (Fig. 4a, S53–S60 and Table S8† for full spectral data at 5 °C). This indicates slower interconversion between conformers, in contrast to the unconstrained peptide. We have observed such behavior previously for constrained peptides that target helical interfaces.[39] To further probe the

effect of the constraint in TACC3$_{518-532-L/R-Bph-IF/fP}$, we carried out ^{1}H variable temperature (VT) NMR experiments from 5–50 °C (Fig. S61 and S62†). Upon gradually increasing the temperature we measured a progressive shift to higher signal intensities (Fig. 4a), improved spatial resolution, and resonance narrowing, confirming that exchange between conformers occurs at low temperatures. TOCSY/NOESY spectra of TACC3$_{518-532-L/R-Bph-IF/fP}$ revealed similar structural features to those found for the WT peptide, and were indicative of a disordered/random-coil structure based on ^{1}H$_{NH}$ and δ_{RC} chemical shifts (Table S10, Fig. S50–S52†); however, some key differences were observed. Firstly, we observed a clear conformational bias at the *trans*-(4-F)Pro528^{TACC3} residue in the constrained peptide towards the desired *exo*-pucker/*trans*-amide population that persisted even at room temperature $(K_{exo/endo}$ (5 °C) = 2.04; $K_{exo/endo}$ (25 °C) = 1.22; insets Fig. 4a and Table S11†). Secondly, we observed more extensive nOe correlations for Phe525^{TACC3}. Spectral correlations for the WT unconstrained peptide indicate Phe525^{TACC3} contacts both the N-terminal residue (Ser524^{TACC3}) and the C-terminal residues (Asp527^{TACC3}, Pro528^{TACC3}) (Fig. S38–S41†), whereas for TACC3$_{518-532-L/R-Bph-IF/fP}$ the correlations were consistent with preferential orientation towards the N-terminus (Glu522^{TACC3} and Ser524^{TACC3}, Fig. 4b, c, S58–S60†). These results indicate that whilst Phe525^{TACC3} freely rotates about the C$_\alpha$–C$_\beta$ dihedral in the WT sequence, in the constrained peptide its orientation is biased to that observed when bound to Aurora-A. We also examined the constrained variant TACC3$_{518-532-L/R-Bph}$, where the (4-I)Phe525 and *trans*-(4-F)Pro528 are not present (Tables S12, 13,† Fig. S63–S71†). We
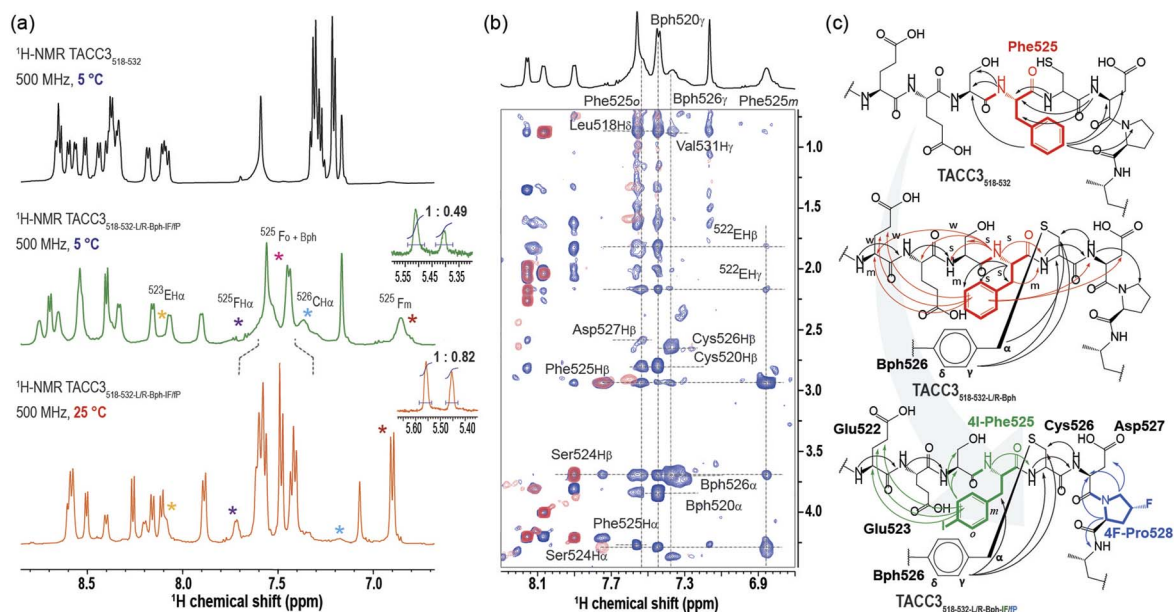

Fig. 4 NMR secondary structure analysis of TACC3$_{518-532}$ and constrained TACC3$_{518-532\_Bph\_LR\_IF/fP}$: (a) ^{1}H-NMR spectra of TACC3$_{518-532}$ (in black) and TACC3$_{518-532\_L/R\_Bph\_IF/fP}$ (in green) showing the amide-bond region of the peptides as observed at 5 °C; shown in orange is the ^{1}H-NMR spectra of TACC3$_{518-532\_L/R\_Bph\_IF/fP}$ as observed at 25 °C; (b) superposition of the ^{1}H–^{1}H TOCSY (in red) and ^{1}H–^{1}H NOESY spectra (in blue) at the NH-Hα region of constrained TACC3$_{518-532\_L/R\_Bph\_IF/fP}$; (c) schematics showing the comparative intramolecular spatial ^{1}H–^{1}H NOESY contacts and the phenylalanine aromatic ring orientation as observed within TACC3$_{518-532}$ WT, control constrained TACC3$_{518-532\_L/R\_Bph}$ and TACC3$_{518-532\_Bph\_LR\_IF/fP}$. All samples as measured in buffer/D$_2$O 90/10% vol/vol. Buffer: 25 mM potassium phosphate, 50 mM NaCl, 5 mM MgCl$_2$, pH = 7.5.

observed intermediate behavior for this peptide (Fig. 4c), with nOe correlations between residues on either side of Phe525, but with higher intensity for N-terminal residues. Finally, we analyzed our second constrained model peptide, TACC3$_{518-532-S/E-Bph}$ (Tables S14, S15, Fig. S72–S80†) and TACC3$_{518-532-S/E-Bph-IF/fP}$ (Tables S16, 17, Fig. S81–S89†). Results from these experiments were consistent with those observed for TACC3$_{518-532-L/R-Bph-IF/fP}$, showing for the S/E Bph-constrained peptide a similar random-coil structure (Table S17, Fig. S50–52†), orientational bias of Phe525^{TACC-} towards the N-terminus (Fig. S86–S89†) and bias of the *trans*-(4-F)Pro528 residue towards the *exo*-pucker/*trans*-amide configuration ($K_{exo/endo} = 2.70$, Table S11, Fig. S90 and S91†).

Taken together, these NMR data indicate a combination of all three modifications restricts the conformational ensemble in the constrained peptidomimetics, presumably disfavouring some that are unproductive for binding and in effect predisposing the peptides towards higher affinity Aurora-A binding.

2.6 Enhanced binding of peptidomimetics to Aurora-A is entropically driven

Whilst the NMR analyses indicated that the constrained peptidomimetics are conformationally more restricted in comparison to the linear variant, they also indicated the constrained peptide ensemble has a largely disordered/random-coil conformation. To explore how restricting the accessible conformations influences the thermodynamics of binding, we carried out isothermal titration calorimetry (ITC) experiments (Fig. 5 and Table S18†). By comparing the individual contributions of enthalpy and entropy for the interaction of constrained and unconstrained TACC3 variants to Aurora-A (Fig. 5), the constrained variants (*e.g.* TACC3$_{518-532-LR-Bph-IF/fP}$ $-T\Delta S = -22.7$ kJ mol^{-1}) were observed to exhibit a more favorable entropy of binding in comparison to the linear variants (TACC3$_{522-536}$ $-T\Delta S = -2.7$ kJ mol^{-1}, TACC3$_{518-532}$ $T\Delta S = -15.0$ kJ mol^{-1}; Fig. S92–S96†). This is compensated by a less favorable enthalpic contribution to binding (TACC3$_{518-532}$ $\Delta H = -10.6$ kJ mol^{-1} constrained variants $\Delta H \sim -7.2$–8.5 kJ mol^{-1}).[9,45,46]

To further assess the thermodynamic determinants of binding, we performed variable-temperature fluorescence anisotropy experiments (Fig. S97–S98†) and Van't Hoff analyses under different conditions, specifically: buffer (Tris, HEPES), pH (pH = 6.0, 7.5 and 8.0) and salt content (NaCl = 0 mM, 150 mM). Although we observed subtle differences in absolute values of $-T\Delta S$ and ΔH, the observed trends were consistent with the ITC experiments (*i.e.* more favorable $-T\Delta S$ and less favorable ΔH for the constrained *versus* unconstrained peptide), indicating that the thermodynamic differences between unconstrained peptide and constrained peptidomimetic may be attributed to the constraint.

2.7 TACC3$_{518-532}$ peptidomimetics stimulate Aurora-A activity

As an incomplete kinase,[26,27] control of Aurora-A localization and activation is achieved through interaction with its intrinsically disordered clients. Indeed, TACC3 behaves as an allosteric activator of Aurora-A, whereby the protein binds to and activates the kinase, then in turn is phosphorylated, and recruited to microtubules.[27] Such client/Aurora-A interactions cover a significant surface area on the kinase and so delineating the minimal structural determinants and changes needed to promote kinase activity is challenging. Similarly, orthosteric inhibitors of Aurora-A PPIs that simultaneously inactivate the kinase are unlikely to be differentiated from active site kinase inhibitors. We therefore assessed the effect of the peptidomimetics on Aurora-A kinase activity by performing Aurora-A autophosphorylation experiments *in vitro* (Fig. 6a). When unphosphorylated Aurora-A was incubated in the presence of the constrained peptides and ATP, they were found to stimulate Aurora-A kinase activity more effectively when compared to the WT unconstrained control peptide, with the effect being qualitatively more pronounced for the L/R constrained variants.
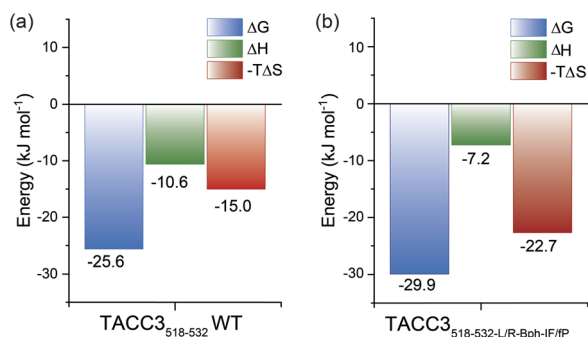

Fig. 5 Thermodynamics of binding in the presence of Aurora-A: (a) ITC thermodynamic signatures of linear TACC3$_{518-532}$; (b) constrained TACC3$_{518-532-L/R-Bph-I/fP}$ binding to Aurora-A$_{122-403-C290A/C393A}$. Data is shown as the average ± SD of two independent titrations of the protein (46 μM) in 25 mM Tris buffer, 150 mM NaCl, 5 mM MgCl$_2$, 5% v/v glycerol at pH 7.5.
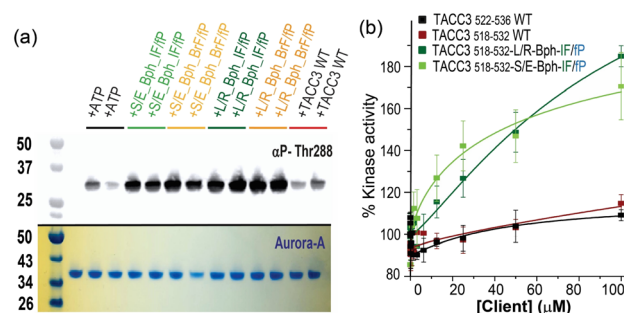

Fig. 6 Kinase activation by peptidomimetics (a) qualitative kinase assay monitoring the autophosphorylation of unphosphorylated Aurora-A in the presence of TACC3$_{522-536}$ and constrained peptides (all peptides 10 μM). Incubates were analyzed by SDS–PAGE (lower panel) and western-blotted with an α-phospho-T288 Aurora-A antibody (upper panel); (b) % kinase activation of Aurora-A (10 nM) in the presence of linear and constrained TACC3 peptides. ADP-Glo luminescence signal was normalized to the protein-only activity after subtracting the background signal. Shown are the means ± SD at each concentration of the peptides from duplicate experiments.

ADP-Glo assays provided further quantitative data on the phosphorylation activity of the protein (10 nM) in the presence of excess substrate (kemptide; 100 μM) at increasing concentrations of the linear and constrained peptides (Fig. 6b, note the acetylated peptides are used and full saturation of Aurora A may not occur at maximal peptide concentrations on the basis of the affinities determined by ITC). These experiments illustrate that both linear WT variants are relatively poor activators of the kinase, whereas the constrained peptidomimetics stimulate Aurora-A and promote substrate phosphorylation in a dose-dependent manner by up to 160–190%. A mass spectrometry kinetic assay for kemptide phosphorylation corroborated these results (Fig. S99†). Importantly, whilst TACC3$_{519-563}$ was previously shown to activate Aurora-A,[26,27] the effects with the shorter truncated TACC3$_{522-536}$, and TACC3$_{518-532}$ used here are small, implying that other features in the longer TACC3 sequence can play a role in activation of Aurora. In contrast the modified and truncated peptides (e.g., TACC3$_{518-532-LR-Bph-IF/fP}$) have a more pronounced effect in activating the kinase, unveiling a "minimal activation motif" that is enough for activation but only if binding is sufficiently potent.

2.8 Constrained TACC3$_{518-532-L/R-Bph-I/fP}$ acts as an allosteric inhibitor of the N-Myc/Aurora-A interaction

We finally assessed if the increase in potency was gained at the expense of binding pocket specificity. We therefore tested TACC3$_{518-532-L/R-Bph-IF/fP}$ in FA competition experiments against TPX2 and N-Myc (Fig. 7). Similarly to TACC3, TPX2$_{1-43}$ has been shown to bind Aurora-A at the N-lobe of the protein. However, it binds to the opposing face, via two separate segments linked by a disordered region that can interact and insert into the W, F and Y pockets on Aurora-A (Fig. 7a, TPX2$_{1-43}$; PDB: 1OL5).[47] On the other hand, N_Myc has been shown to bind between the N- and C-lobes to a groove adjacent to the activation loop of the kinase (N-Myc$_{61-89}$; PDB: 5G1X).[48] In FA competition assays, the constrained peptidomimetics exhibited limited evidence of TPX2 displacement (IC$_{50}$ ≫ 200 μM versus TPX2$_{7-43}$ IC$_{50}$, = 20 ± 1 μM; see Fig. S100†) indicating promising specificity for the TACC3 binding site. More surprisingly, the constrained variants were observed to out-compete N-Myc (Fig. 7c and S101†). The most potent constrained variant (TACC3$_{518-532-L/R-Bph-I/fP}$ IC$_{50}$ = 28 ± 1 μM) was more potent than the control N-Myc sequence (N-Myc$_{61-89}$, IC$_{50}$ = 56 ± 5 μM). To assess if these observations
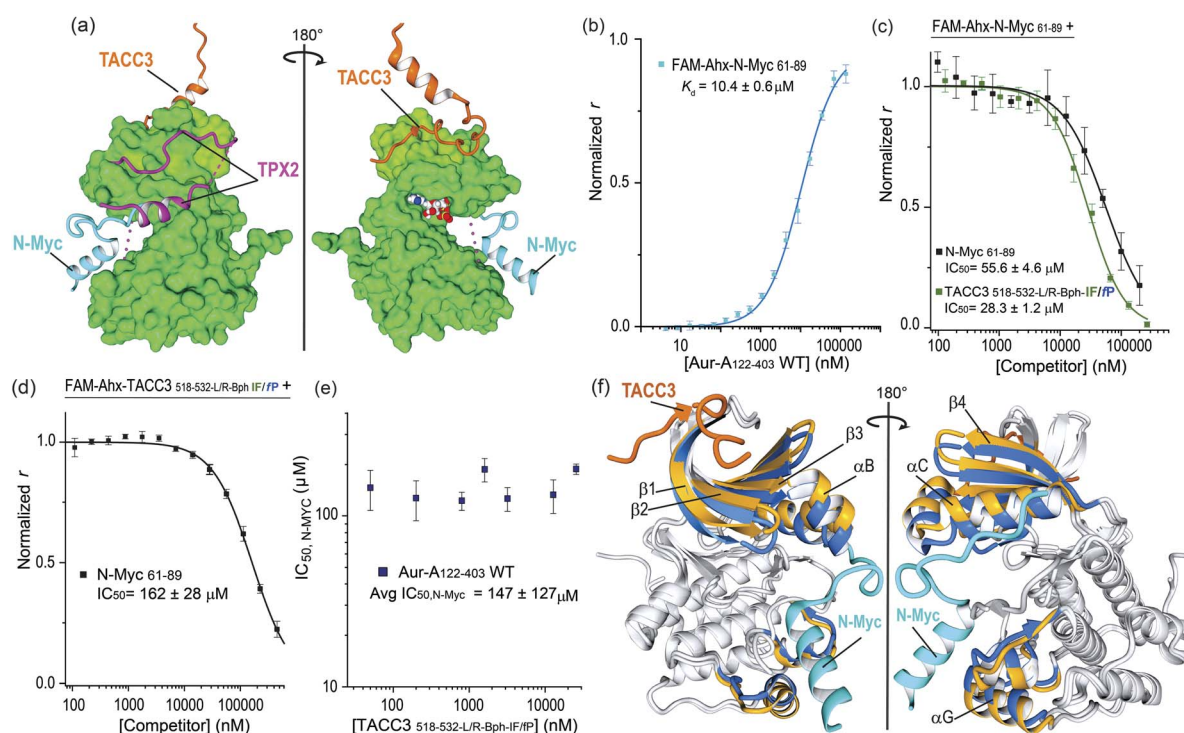

Fig. 7 Constrained TACC3$_{518-532-LR-Bph-IF/fP}$ as an allosteric inhibitor of N-Myc/Aurora-A PPI: (a) MUSTANG-aligned X-ray crystal structures of TACC3/Aurora-A complex (PDB: 5ODT), TPX2 (PDB: 1OL5), and N-Myc (PDB: 5G1X) showing their binding regions. For representation, only the Aurora-A molecule present in the TACC3/Aurora-A structure is shown; (b) direct FA titration of fluorescently-labeled FAM-Ahx-N-Myc$_{61-89}$ (50 nM) with Aurora-A$_{122-403-C290A/C393A}$; (c) FA competition assay of control N-Myc$_{61-89}$ (black line) and constrained TACC3$_{518-532-LR-Bph-IF/fP}$ (forest green) peptides against FAM-Ahx-N-Myc$_{61-89}$ (200 nM) in the presence of Aurora-A$_{122-403-C290A/C393A}$; (d) FA competition assay of N-Myc$_{61-89}$ against fluorescently-labeled constrained FAM-Ahx-TACC3$_{518-532-LR-Bph-IF/fP}$ (200 nM) in the presence of Aurora-A$_{122-403-C290A/C393A}$; (e) completion FA N-Myc IC$_{50}$'s values measured for N-Myc$_{61-89}$ against fluorescently-labeled TACC3$_{518-532-LR-Bph-IF/fP}$ at increased concentrations of the tracer and constant protein concentration; (f) MUSTANG-aligned X-ray crystal structures of TACC3/Aurora-A (PDB: 5ODT; TACC3 shown in orange; Aurora-A in grey) and N-Myc/Aurora-A complexes (PDB: 5G1X; N-Myc shown in blue; Aurora-A in grey). For comparison, highlighted in color are beta-sheets β1–β4 and helices αB, αC and αG in Aurora-A structures when bound to TACC3 (shown in gold) or to N-Myc (shown in cyan). All FA competition data and derived IC$_{50}$ values are given as the means ± SD of a triplicate assay at a constant concentration of the protein (5 μM) in 25 mM Tris, 150 mM NaCl, 5 mM MgCl$_2$, pH 7.5, 25 °C.

could be the consequence of orthosteric competition for the N-Myc binding site we performed the reverse experiment where acetylated N-Myc$_{61-89}$ was employed to displace fluorescently-labeled TACC-3$_{518-532-L/R-Bph-I/fP}$ (Fig. 7d). This N-Myc sequence was also observed to out-compete the TACC3 peptide.

An allosteric mode of inhibition is characterized by the competitor binding at a separate site from that of the "substrate–ligand", and showing similar affinity for the target regardless of the presence of the substrate-ligand.[49–51] Under this model the dose/response IC$_{50}$ values observed for a competitor should remain constant regardless of the ligand concentration. To probe further the role of allostery, we performed FA competition assays at varying concentrations of FAM-labelled TACC3$_{518-532-L/R-Bph-IF/fP}$ (0.05–25.6 μM, Fig. S102†); performing the opposing experiment i.e. displacing varying concentrations of FAM-N-Myc$_{61-89}$, was not practical due to the significantly weaker binding of N-Myc for Aurora-A. The N-Myc IC$_{50}$ values at each tracer concentration did not vary markedly (IC$_{50}$ ~ 120–160) μM (Fig. 7e) confirming an allosteric mode of inhibition.

Analysis of the crystal structures reported for Aurora-A in the presence of TACC3 and N-Myc offers a rationale for the allosteric inhibition. Numerous, conformational changes in the protein upon binding each substrate are observed (Fig. 7f). The N-lobe sheets β1–β3 and helices α$_B$–α$_C$ show a significant deviation in their relative positions between both structures, and the deviation appears to be conformationally transmitted to αG helix in the C-lobe, which is directly involved in N-Myc binding. The displacement in β1-β3 and helices αB–αC in the TACC3/Aurora-A structure, when compared to that of N-Myc, was also observed in a recently reported CEP192/Aurora-A structure. Notably, binding of CEP192 only to the TACC3 site on Aurora-A stimulates kinase activity, consistent with a conserved function through a similar allosteric mechanism.[52]

3 Conclusions

Herein we have described a rational approach to the development of competitive peptidomimetic inhibitors, e.g. TACC3$_{518-}$

Fig. 8 Thermodynamics of binding in the presence of Aurora-A. Diagram schematically illustrating the hypothetical free energy profile of a one-step/one-barrier peptide-protein binding event for a linear (a) and a constrained peptide (b).

532-L/R-Bph-IF/fP, of the TACC3/Aurora-A interaction. Key to the success of this approach was the incorporation of a constraint within the peptide despite the absence of a well-defined secondary structure at the interface. Whilst a structurally well-defined interaction between TACC3/Aurora-A occurs and must be replicated in large part by the peptidomimetic, the unbound form of both the peptide and the constrained peptidomimetic were shown to be largely disordered. The enhanced affinity of the constrained peptidomimetic arises from a restricted conformational space, in effect raising the energy of the ensemble and resulting in a more favourable entropy of binding to the kinase (Fig. 8). Related effects have been observed whereby subtle changes to a 14-3-3 binding macrocycle can bias a conformational ensemble towards the bound conformation as demonstrated through free energy perturbation and molecular dynamics analyses.[53] The behavior observed here is also similar to that recently described to occur upon methylation of backbone amides for a ligand that recognizes its target through β-strand complementation.[10] Raising the energy of the unbound ensemble can offer a general route to enhancing target binding affinity as opposed to preorganizing a ligand in its bound conformation – a difficult prospect given PPIs occur as partially bound states.[46] Promisingly, the high affinity of the most potent peptidomimetic TACC3$_{518-532-L/R-Bph-IF/fP}$ opens up new opportunities to understand and allosterically regulate the function and interactions of Aurora-A. A number of Aurora-A interactors e.g. TACC3 (ref. 26) and TPX2 (ref. 54) activate the kinase, despite binding at different sites, whilst paradoxically CEP192,[55] which binds at both TACC3 and TPX2 sites, suppresses kinase activity. All three proteins may participate in additional non-covalent interaction with the kinase beyond that revealed by their X-ray structures, complicating an interpretation of the minimal determinants for allosteric kinase modulation. In contrast our minimal peptidomimetics of only thirteen residues are sufficient to induce conformational changes needed to activate the kinase by binding only a single pocket on the N-lobe. This "minimal activation motif" relies on the more potent binding of the peptidomimetic in contrast to the native sequence.

The more potent peptidomimetic also allosterically displaces N-Myc from its binding site and does so more effectively that the native sequence; this allosteric displacement is likely linked by common structural changes that lead to kinase activation. Inhibition of the N-Myc/Aurora-A interaction[39] may represent a target for anticancer drug-development – a number of active-site ligands have been shown to allosterically displace N-Myc,[48,56] but may prove problematic as a consequence of downregulating the essential functions of Aurora-A.[57,58] Being able to orthosterically inhibit the TACC3/Aurora-A interaction and allosterically inhibit N-Myc/Aurora-A without inhibiting kinase activity may thus represent a promising alternative to these active-site ligands. Further efforts towards this goal would need to establish the extent to which allosteric N-Myc displacement and Aurora-A activation can be balanced. Thus, these peptidomimetic tools inform on allosteric regulation in Aurora A and reveal new opportunities for chemical probe development.
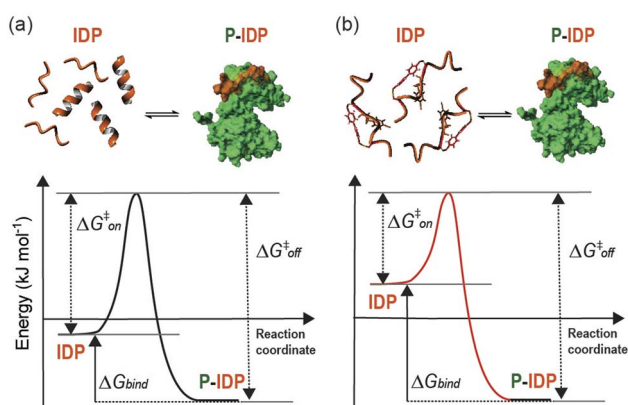
Data availability

All relevant data are included in the ESI.†

Author contributions

A. J. W. conceived and designed the research program, with the input of M. H. W and R. B.; D. G. designed the studies and performed the research, with support from M. W. J. A. M. performed the kinase autophosphorylation assays *in vitro* and contributed to protein production. A. J. W and D. G. wrote the manuscript with contributions from all authors.

Conflicts of interest

There are no conflicts to declare.

Acknowledgements

Notes and references

1 M. A. Skinnider, N. E. Scott, A. Prudova, C. H. Kerr, N. Stoynov, R. G. Stacey, Q. W. T. Chan, D. Rattray, J. Gsponer and L. J. Foster, *Cell*, 2021, **184**, 4073–4089.

2 P. Braun and A.-C. Gingras, *Proteomics*, 2012, **12**, 1478–1498.

3 D. E. Scott, A. R. Bayly, C. Abell and J. Skidmore, *Nat. Rev. Drug Discovery*, 2016, **15**, 533–550.

4 M. R. Arkin, Y. Tang and J. A. Wells, *Chem. Biol.*, 2014, **21**, 1102–1114.

5 A. J. Wilson, *Chem. Soc. Rev.*, 2009, **38**, 3289–3300.

6 *Inhibitors of Protein–Protein Interactions: Small Molecules, Peptides and Macrocycles*, ed. A. Tavassoli, Royal Society of Chemistry, London, vol. 17, 2020.

7 M. Pelay-Gimeno, A. Glas, O. Koch and T. N. Grossmann, *Angew. Chem., Int. Ed.*, 2015, **54**, 8896–8927.

8 M. Muttenthaler, G. F. King, D. J. Adams and P. F. Alewood, *Nat. Rev. Drug Discovery*, 2021, **20**, 309–325.

9 H. Wang, R. S. Dawber, P. Zhang, M. Walko, A. J. Wilson and X. Wang, *Chem. Sci.*, 2021, **12**, 5977–5993.

10 E. E. Cawood, E. Baker, T. A. Edwards, D. N. Woolfson, T. K. Karamanos and A. J. Wilson, *Chem. Sci.*, 2024, **15**, 10237–10245.

11 Z. C. Adams, A. P. Silvestri, S. Chiorean, D. T. Flood, B. P. Balo, Y. Shi, M. Holcomb, S. I. Walsh, C. A. Maillie, G. K. Pierens, S. Forli, K. J. Rosengren and P. E. Dawson, *ACS Cent. Sci.*, 2023, **9**, 648–656.

12 M. C. Hammond, B. Z. Harris, W. A. Lim and P. A. Bartlett, *Chem. Biol.*, 2006, **13**, 1247–1251.

13 T. R. Siegert, M. J. Bird, K. M. Makwana and J. A. Kritzer, *J. Am. Chem. Soc.*, 2016, **138**, 12876–12884.

14 Y. Huang, M. M. Wiedmann and H. Suga, *Chem. Rev.*, 2019, **119**, 10360–10391.

15 K. Deyle, X.-D. Kong and C. Heinis, *Acc. Chem. Res.*, 2017, **50**, 1866–1874.

16 A. Glas, D. Bier, G. Hahne, C. Rademacher, C. Ottmann and T. N. Grossmann, *Angew. Chem., Int. Ed.*, 2014, **53**, 2489–2493.

17 A. R. Barr and F. Gergely, *J. Cell Sci.*, 2007, **120**, 2987–2996.

18 F. J. Giles, J. Cortes, D. Jones, D. Bergstrom, H. Kantarjian and S. J. Freedman, *Blood*, 2007, **109**, 500–502.

19 M. Amin, S. E. Minton, P. M. LoRusso, S. S. Krishnamurthi, C. A. Pickett, J. Lunceford, D. Hille, D. Mauro, M. N. Stein, A. Wang-Gillam, L. Trull and A. C. Lockhart, *Invest. New Drugs*, 2016, **34**, 84–95.

20 S. Lheureux, A. Tinker, B. Clarke, P. Ghatage, S. Welch, J. I. Weberpals, N. C. Dhani, M. O. Butler, K. Tonkin, Q. Tan, D. S. P. Tan, K. Brooks, J. Ramsahai, L. Wang, N.-A. Pham, P. A. Shaw, M. S. Tsao, S. Garg, T. Stockley and A. M. Oza, *Clin. Cancer Res. Off. J. Am. Assoc. Cancer Res.*, 2018, **24**, 6168–6174.

21 O. A. O'Connor, M. Özcan, E. D. Jacobsen, J. M. Roncero, J. Trotman, J. Demeter, T. Masszi, J. Pereira, R. Ramchandren, A. Beaven, D. Caballero, S. M. Horwitz, A. Lennard, M. Turgut, N. Hamerschlak, F. A. d'Amore, F. Foss, W.-S. Kim, J. P. Leonard, P. L. Zinzani, C. S. Chiattone, E. D. Hsi, L. Trümper, H. Liu, E. Sheldon-Waniga, C. D. Ullmann, K. Venkatakrishnan, E. J. Leonard, A. R. Shustov and Lumiere Study Investigators, *J. Clin. Oncol. Off. J. Am. Soc. Clin. Oncol.*, 2019, **37**, 613–623.

22 E. Manchado, M. Guillamot and M. Malumbres, *Cell Death Differ.*, 2012, **19**, 369–377.

23 A. S. Nikonova, I. Astsaturov, I. G. Serebriiskii, R. L. Dunbrack and E. A. Golemis, *Cell. Mol. Life Sci.*, 2013, **70**, 661–687.

24 F. Zheng, C. Yue, G. Li, B. He, W. Cheng, X. Wang, M. Yan, Z. Long, W. Qiu, Z. Yuan, J. Xu, B. Liu, Q. Shi, E. W.-F. Lam, M.-C. Hung and Q. Liu, *Nat. Commun.*, 2016, **7**, 10180.

25 B. Adhikari, J. Bozilovic, M. Diebold, J. D. Schwarz, J. Hofstetter, M. Schröder, M. Wanior, A. Narain, M. Vogt, N. Dudvarski Stankovic, A. Baluapuri, L. Schönemann, L. Eing, P. Bhandare, B. Kuster, A. Schlosser, S. Heinzlmeir, C. Sotriffer, S. Knapp and E. Wolf, *Nat. Chem. Biol.*, 2020, **16**, 1179–1188.

26 S. G. Burgess, M. Mukherjee, S. Sabir, N. Joseph, C. Gutiérrez-Caballero, M. W. Richards, N. Huguenin-Dezot, J. W. Chin, E. J. Kennedy, M. Pfuhl, S. J. Royle, F. Gergely and R. Bayliss, *EMBO J.*, 2018, **37**, e97902.

27 S. G. Burgess, I. Peset, N. Joseph, T. Cavazza, I. Vernos, M. Pfuhl, F. Gergely and R. Bayliss, *PLOS Genet.*, 2015, **11**, e1005345.

28 G.-H. Ha, J.-L. Kim and E.-K. Y. Breuer, *Cancer Lett.*, 2013, **336**, 24–33.

29 R. Costa, B. A. Carneiro, T. Taxter, F. A. Tavora, A. Kalyan, S. A. Pai, Y. K. Chae and F. J. Giles, *Oncotarget*, 2016, **7**, 55924–55938.

30 P. J. LeRoy, J. J. Hunter, K. M. Hoar, K. E. Burke, V. Shinde, J. Ruan, D. Bowman, K. Galvin and J. A. Ecsedy, *Cancer Res.*, 2007, **67**, 5362–5370.

31 M. G. Manfredi, J. A. Ecsedy, K. A. Meetze, S. K. Balani, O. Burenkova, W. Chen, K. M. Galvin, K. M. Hoar, J. J. Huck, P. J. LeRoy, E. T. Ray, T. B. Sells, B. Stringer, S. G. Stroud, T. J. Vos, G. S. Weatherhead, D. R. Wysong, M. Zhang, J. B. Bolen and C. F. Claiborne, *Proc. Natl. Acad. Sci. U. S. A.*, 2007, **104**, 4106–4111.

32 A. Lioutas and I. Vernos, *EMBO Rep.*, 2013, **14**, 829–836.

33 P. Singh, G. E. Thomas, K. K. Gireesh and T. K. Manna, *J. Biol. Chem.*, 2014, **289**, 31719–31735.

34 C. W. Wood, A. A. Ibarra, G. J. Bartlett, A. J. Wilson, D. N. Woolfson and R. B. Sessions, *Bioinformatics*, 2020, **36**, 2917–2919.

35 R. W. Newberry and R. T. Raines, *Top. Heterocycl. Chem.*, 2017, **48**, 1–25.

36 M. L. DeRider, S. J. Wilkens, M. J. Waddell, L. E. Bretscher, F. Weinhold, R. T. Raines and J. L. Markley, *J. Am. Chem. Soc.*, 2002, **124**, 2497–2505.

37 P. Zhang, M. Walko and A. J. Wilson, *Chem. Commun.*, 2023, **59**, 1697–1700.

38 P. Zhang, M. Walko and A. J. Wilson, *Bioorg. Med. Chem. Lett.*, 2023, **87**, 129260.

39 R. S. Dawber, D. Gimenez, M. Batchelor, J. A. Miles, M. H. Wright, R. Bayliss and A. J. Wilson, *ChemBioChem*, 2024, **25**, e202300649.

40 L. Gentilucci, R. De Marco and L. Cerisoli, *Curr. Pharm. Des.*, 2010, **16**, 3185–3203.

41 L. J. Smith, K. M. Fiebig, H. Schwalbe and C. M. Dobson, *Folding Des.*, 1996, **1**, R95–R106.

42 M. Kjaergaard and F. M. Poulsen, *J. Biomol. NMR*, 2011, **50**, 157–165.

43 D. S. Wishart and B. D. Sykes, *J. Biomol. NMR*, 1994, **4**, 171–180.

44 M. Batchelor, M. Wolny, E. G. Baker, E. Paci, A. P. Kalverda and M. Peckham, *J. Biol. Chem.*, 2019, **294**, 3219–3234.

45 J. A. Miles, D. J. Yeo, P. Rowell, S. Rodriguez-Marin, C. M. Pask, S. L. Warriner, T. A. Edwards and A. J. Wilson, *Chem. Sci.*, 2016, **7**, 3694–3702.

46 C. A. Hunter and S. Tomas, *Chem. Biol.*, 2003, **10**, 1023–1032.

47 R. Bayliss, T. Sardon, I. Vernos and E. Conti, *Mol. Cell*, 2003, **12**, 851–862.

48 M. W. Richards, S. G. Burgess, E. Poon, A. Carstensen, M. Eilers, L. Chesler and R. Bayliss, *Proc. Natl. Acad. Sci. U. S. A.*, 2016, **113**, 13726–13731.

49 J. Jakubík, A. Randáková, N. Chetverikov, E. E. El-Fakahany and V. Doležal, *Sci. Rep.*, 2020, **10**, 14421.

50 C. Yung-Chi and W. H. Prusoff, *Biochem. Pharmacol.*, 1973, **22**, 3099–3108.

51 A. Christopoulos and T. Kenakin, *Pharmacol. Rev.*, 2002, **54**, 323–374.

52 J.-G. Park, H. Jeon, S. Shin, C. Song, H. Lee, N.-K. Kim, E. E. Kim, K. Y. Hwang, B.-J. Lee and I.-G. Lee, *Sci. Adv.*, **9**, eadf8582.

53 K. Wallraven, F. L. Holmelin, A. Glas, S. Hennig, A. I. Frolov and T. N. Grossmann, *Chem. Sci.*, 2020, **11**, 2269–2276.

54 R. Bayliss, T. Sardon, J. Ebert, D. Lindner, I. Vernos and E. Conti, *Cell Cycle*, 2004, **3**, 402–405.

55 J. Holder, J. A. Miles, M. Batchelor, H. Popple, M. Walko, W. Yeung, N. Kannan, A. J. Wilson, R. Bayliss and F. Gergely, *EMBO J.*, 2024, **43**, 5381–5420.

56 W. C. Gustafson, J. G. Meyerowitz, E. A. Nekritz, J. Chen, C. Benes, E. Charron, E. F. Simonds, R. Seeger, K. K. Matthay, N. T. Hertz, M. Eilers, K. M. Shokat and W. A. Weiss, *Cancer Cell*, 2014, **26**, 414–427.

57 R. Katayama, A. T. Shaw, T. M. Khan, M. Mino-Kenudson, B. J. Solomon, B. Halmos, N. A. Jessop, J. C. Wain, A. T. Yeo, C. Benes, L. Drew, J. C. Saeh, K. Crosby, L. V. Sequist, A. J. Iafrate and J. A. Engelman, *Sci. Transl. Med.*, 2012, **4**, 120ra17.

58 D. Gupta, M. Kumar, S. Saifi, S. Rawat, A. S. Ethayathulla and P. Kaur, *Int. J. Biol. Macromol.*, 2024, **265**, 130913.